11. S. Barnett, P. Radmore, *Methods in Theoretical Quantum Optics* (Oxford Univ. Press, Oxford, 1997).
12. P. Hariharan, *Basics of Interferometry* (Academic Press, New York, 1992).
13. The nonscattering term depends on the total scattering rate over all angles (a function of *r*) and can be derived from the optical theorem (*19*). Additional considerations of scattering efficiency are straightforward and only affect the rate of localization.
14. S. M. Tan, D. F. Walls, *Phys. Rev. A* **47**, 4663 (1993).
15. U. Eichmann *et al.*, *Phys. Rev. Lett.* **70**, 2359 (1993).
16. M. Tegmark, J. A. Wheeler, *Sci. Am.* **284**, 68 (2001).
17. J. Javanainen, S. M. Yoo, *Phys. Rev. Lett.* **76**, 161 (1996).
18. J. A. Dunningham, K. Burnett, *Phys. Rev. Lett.* **82**, 3729 (1999).
19. L. Schiff, *Quantum Mechanics* (McGraw Hill, New York, 1968).

20. We thank A. R. P. Rau and W. D. Phillips for many helpful discussions. Supported by the National Science Foundation; the Marshall Aid Commemoration Commission; Merton College, Oxford; the UK Engineering and Physical Sciences Research Council; The Royal Society and Wolfson Foundation; and the European Union through the Cold Quantum Gases network.

24 March 2003; accepted 10 July 2003

Spectroscopic Identification of Carbonate Minerals in the Martian Dust

Joshua L. Bandfield,* Timothy D. Glotch, Philip R. Christensen

Thermal infrared spectra of the martian surface indicate the presence of small concentrations (~2 to 5 weight %) of carbonates, specifically dominated by magnesite ($MgCO_3$). The carbonates are widely distributed in the martian dust, and there is no indication of a concentrated source. The presence of small concentrations of carbonate minerals in the surface dust and in martian meteorites can sequester several bars of atmospheric carbon dioxide and may have been an important sink for a thicker carbon dioxide atmosphere in the martian past.

Carbonate minerals play an important role in determining the history of the martian atmosphere, geology, and hydrology. Specifically, carbonate minerals provide a trace for the presence of liquid water in the martian past and form readily in a CO_2 atmosphere when water is present (*1*, *2*). Carbonate minerals are also a potential sink of atmospheric CO_2 because there is no known widespread carbonate-recycling mechanism present on Mars such as plate tectonics on Earth. This sink may have important implications as regards the fate of a potentially thicker past martian atmosphere. Determining the quantity, form, and distribution of carbonate minerals on Mars is key to a basic understanding of the evolution of water and the atmosphere and to determining local climatic conditions in the martian past suitable for sustaining life.

Carbonate minerals have unique absorptions throughout the near-infrared and thermal infrared spectral regions (*3*–*6*) with overtone and combination bands at 2.35, 2.55, and 4.0 μm, and fundamental absorptions near 7, 11, and 30 μm. However, definitive identification of carbonate minerals on Mars has remained elusive (*7*–*10*).

Researchers used the Viking labeled release experiment to limit the concentration of carbonates present in the martian soil to levels near 1 to 2% in the presence of smectite clays (*11*, *12*). These low levels, as well as the lack of spectroscopic evidence for carbonates, have driven investigations of mechanisms such as ultraviolet photodissociation and acid-fog weathering (*13*, *14*) that may be responsible for the lack of carbonate minerals on Mars. Carbonate minerals have been found in low concentrations (up to ~1 weight %) in several martian meteorites (*15*), indicating that they must be present at some locations on Mars.

The systematic coverage, radiometric accuracy, and multiple emission angle observations of the Thermal Emission Spectrometer (TES) data have allowed for the isolation of the thermal infrared emissivity spectra of the surface dust (*16*) (Fig. 1). These data allow for characterization of the surface and atmospheric properties and separation of the surface and atmospheric contributions to the spectra (*16*). The multiple emission angle observation data use the aerosol opacity information retrieved from each observation to remove aerosol effects and produce quantitative surface emissivities (*17*).

We selected 21 multiple emission angle sequences from a variety of dust-covered, high-albedo regions between 30°S and 15°N, and the surface emissivity was retrieved (*17*) (Fig. 1). All surface spectra have the same spectral character, including a relatively narrow absorption near 830 cm^{-1} and a broad, deep absorption at >1250 cm^{-1}. A superimposed, narrower emissivity minimum is located near 1580 cm^{-1} with a local emissivity maximum near 1630 cm^{-1}. A prominent convex spectral curve is present from 1450 to 1580 cm^{-1}. There is little to no absorption at frequencies <550 cm^{-1} and between 900 and 1250 cm^{-1}. The standard deviation in the spectral shape of the surfaces is <0.01 from 250 to 1610 cm^{-1} and climbs from 0.01 to 0.02 from 1620 to 1650 cm^{-1} (Fig. 1).

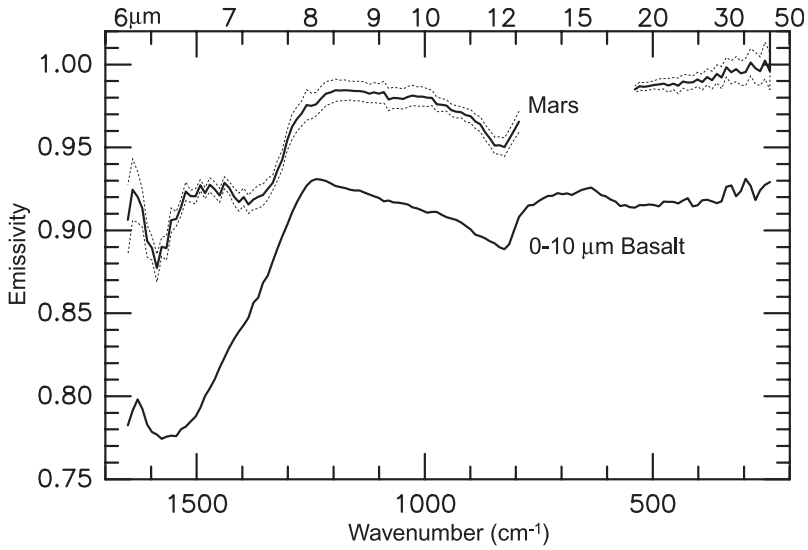

Fig. 1. Mars high-albedo surface dust spectrum (top, solid line) ± SD (dashed lines). A fine-particulate basalt spectrum (solid line, offset) displays similar spectral features from 200 to 1300 cm^{-1} due to its high plagioclase content. Similar to other silicates, sulfates, and oxides, the spectrum does not match well at >1300 cm^{-1}. Bound or adsorbed water is present in the basalt sample, resulting in the emission peak near 1620 cm^{-1}.

Department of Geological Sciences, Arizona State University, Tempe, AZ 85287–6305, USA.

*To whom correspondence should be addressed. E-mail: joshband@asu.edu

The low emissivity values at 830 cm^{-1} and >1250 cm^{-1} are due to fine particulate silicate materials that contain an unknown concentration of plagioclase or zeolites (*16*, *18*). Although the absorption present at >1250 cm^{-1} is consistent with volume scattering effects in fine-particulate silicate materials (*16*, *19*), the spectral shape and depth of the martian dust spectrum require the presence of a material that is highly absorbing at these wave numbers to raise the emissivity (lowering the reflectivity) to the level seen on Mars. The emission peak present at 1630 cm^{-1} indicates the presence of bound or adsorbed water, but the water cannot account for the high emissivities in the martian spectrum from 1350 to 1580 cm^{-1}.

We conducted a systematic laboratory study to determine the composition of the material that is absorbing at high wave numbers in the martian spectrum. A pure 0- to 63-μm-diameter size fraction of labradorite was used as a standard (*17*), and 0- to 63-μm size fractions of different minerals were added at the 10 weight % level to determine their effects on the fine-particulate labradorite spectrum (Fig. 2). Components added included calcite ($CaCO_3$), dolomite [$CaMg(CO_3)_2$], magnesite ($MgCO_3$), siderite ($FeCO_3$), hematite (Fe_2O_3), gypsum ($CaSO_4 \cdot 2H_2O$), and high-silica glass.

The spectral character at wave numbers >1300 cm^{-1} is sensitive to small amounts of the highly absorbing carbonates (<1 weight %) mixed within the weakly absorbing silicates. A high absorption coefficient at these wave numbers is necessary to match both the increased emissivity and unique spectral shape of the Mars surface spectrum (Fig. 2). Only the carbonate minerals and gypsum have any effect on the spectrum of the fine-particulate labradorite (Fig. 2). Bound water in the gypsum approximates the minor emission peak at 1630 cm^{-1}, but not the emissivity increase and convex shape between 1350 and 1580 cm^{-1} seen in the spectra of the martian surface. All of the carbonate components approximate the shape of the martian spectrum between 1250 and 1650 cm^{-1}, including the emissivity minima at 1350 and 1580 cm^{-1} and maxima near 1480 and 1630 cm^{-1} (supporting online text, fig S1).

The high–wave number spectral shape of the spectrum from ~1350 to 1580 cm^{-1} is sensitive and unique to small quantities of carbonate minerals (>0.25 weight %) intimately mixed with silicate minerals in fine-particulate materials (≤74 μm). This property is similar to the 2500 cm^{-1} (4 μm) carbonate absorption that is detectable at small carbonate concentrations (*20*) due to the transparency of silicate minerals. No other common mineral class is highly absorptive in this spectral region, and other oxides, silicates, and sulfates have little influence on the spectral character within this wave number region (supporting online text). The spectral shape between 1350 and 1580 cm^{-1} is unique to materials that contain carbonate minerals, and no other available sample spectrum matches the martian spectrum at these wavelengths.

Carbonate minerals have strong absorptions at ~880 cm^{-1} and between ~300 and 400 cm^{-1}. These absorptions are useful for detecting carbonates in both the atmospheric dust and coarse particulate surfaces in large (≳5%) concentrations. These absorptions are not present or expected to have any detectable effect in fine-particulate mixtures of silicates and carbonates because silicates are highly absorbing in both of these spectral regions. As a result, both materials have roughly similar interactions with light at these wavelengths. In contrast, at wave numbers ≳1300 cm^{-1}, the addition of small amounts (<1%) of carbonates to silicates has detectable effects.

The minimum shifts with the specific composition of the carbonate, from 1540 cm^{-1} for the siderite-component spectrum to 1580 cm^{-1} for the magnesite-component spectrum (Fig. 3). The positions of spectral features in the 1250- to 1650-cm^{-1} range migrate to higher wave numbers with increasing Mg content (Fig. 3), consistent with the positions of their relative absorptions in transmission and emission spectra (*4*, *6*). Other carbonate mineral mixtures may fit the spectra, and the magnesite fit may represent a nonunique solution. Researchers have proposed hydrous carbonates for Mars (*8*) that may be a precursor for the magnesite. We investigated hydromagnesite [$3MgCO_3 \cdot Mg(OH)_2 \cdot 3H_2O$] and found the spectral character to be dissimilar in position, shape, and intensity of its absorptions compared with that of Mars. Although other carbonates can mimic the high–wave number spectral shape of the martian dust spectrum, the magnesite-component spectrum is the only composition that matches the wavelength of the spectral features. The spectral features of dolomite are offset by 20 cm^{-1} and the calcite and dolomite are offset by 40 cm^{-1} from the dust spectrum (Fig. 3).

The particle size distribution can affect the magnitude of the effect of carbonates on the measured spectral features. To estimate the magnitude of this effect, we separated labradorite and magnesite into particle size fractions of 0 to 5, 0 to 10, 10 to 20, 20 to 30, and 30 to 41 μm (*17*). For all particle size fractions, the magnesite component was added to the labradorite in 0.5 weight % increments until the resulting sample spectrum displayed the characteristics present at >1300 cm^{-1} in the martian dust spectrum (*17*). The spectral features could be reproduced with smaller magnesite concentrations for the 0- to 10-μm size fraction relative to the other size fractions (fig. S2).

Most moderate- to high-albedo regions on Mars have a thin (less than a few millimeters) layer of particles with diameters ≤10 μm (*16*, *21*, *22*), probably due to airfall dust. The 0- to 10-μm particle size fraction of the laboratory magnesite-labradorite mixture closely matches this estimate. The spectra of

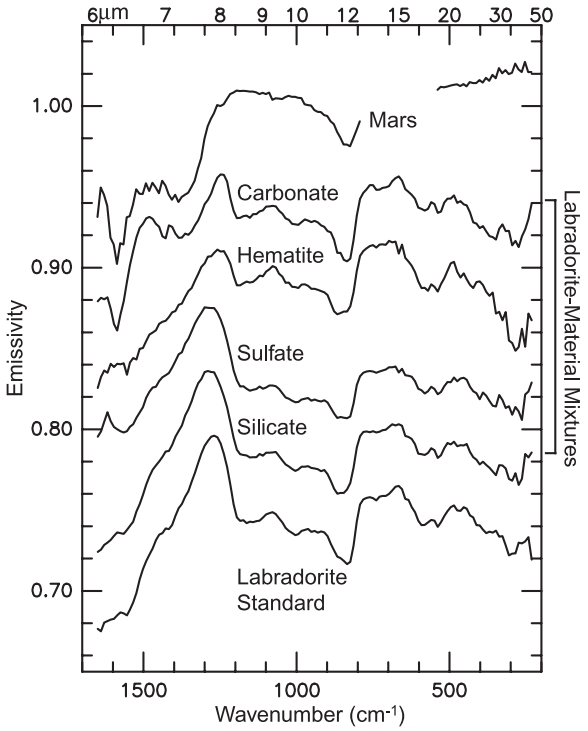

Fig. 2. Mars dust, labradorite standard, and labradorite-material mixture spectra (offset). The spectral shape of labradorite is modified considerably with added carbonate at >1300 cm^{-1}, coincident with a fundamental carbonate absorption. The spectral shape outside this spectral region is not appreciably modified because strong silicate absorptions coincide with the other carbonate absorptions. Only the labradorite-carbonate mixture has a notable effect on the spectral shape, except for a peak present in the labradorite-sulfate mixture at 1640 cm^{-1} due to the bound water in gypsum.

this size fraction displayed the largest change in spectral features due to the addition of small amounts of carbonate, and ≥2 to 3 weight % magnesite mixed with labradorite reproduced the martian spectral features (supporting online text).

Other measurements may place limits on the abundance of carbonates present. The atmospheric dust is probably similar to the material on the surface. The spectral response of the atmospheric dust displays a smooth continuum from 1300 to 1650 cm^{-1} with no apparent absorption features (*16*) that would be detectable if ≳5% carbonate was present in the atmospheric dust (*23*). The detection limit is higher for atmospheric dust because the observation is not as sensitive to the presence of carbonates as the surface dust observation (supporting online text). An upper limit of 5% carbonate on the martian surface has also been determined from near- and mid-infrared spectral measurements (*7*, *9*). Higher concentrations (>10%) of hydrated carbonates may be present and not detected spectrally, because their spectral features are less prominent (*8*).

There is no detectable variation in the shape of the short-wavelength spectral shape within the 21 sites investigated for this study (Fig. 1), probably because the atmosphere transports the dust ubiquitously (*16*). Low-albedo regions display featureless, high (>0.98) emissivities at >1300 cm^{-1}. This is consistent with coarse particulate (≳40 μm) silicate surfaces with <5% carbonate material (*10*, *16*, *24*, *25*). The same concentration of carbonate minerals may be present within coarse particulate surfaces, but the carbonate minerals would be below the detection limit of the TES data.

Carbonate minerals may form under low–CO_2 pressure conditions in which liquid water is not stable but may be present in a transient state (*1*). It is unclear, however, how much, if any, water needs to be present for carbonate formation to take place. Mg and Ca carbonates and oxides should be common and thermodynamically stable weathering products in the present relatively dry and thin martian atmosphere, whereas smectite clays and Ca carbonates would be present if weathering occurred under wetter conditions in a thicker CO_2 atmosphere (*2*).

Carbonate formation can serve as a buffer for the martian atmosphere (*26*, *27*). Carbonates can form at a rapid rate when the martian atmospheric conditions allow for liquid water in a transitory state (*26*). In the presence of unweathered intermediate-to-mafic lithologies, a CO_2 atmosphere, and water, carbonate formation would occur until the atmosphere became thin to the point that the chemical reactions involved in carbonate formation would slow considerably (*2*, *26–30*). Although dependent on a number of factors under actual martian conditions (*27*), carbonate formation could become prohibitively slow at a pressure near the current average martian surface pressure (and the triple point of water) and would resume only with an increase of atmospheric pressure (*26*).

The carbonate minerals present in the martian dust may also have originated from the erosion and dispersal of carbonate-bearing source rocks. Several martian meteorites have small, disseminated concentrations of Mg, Ca, and Fe carbonates that formed by precipitation from water in fractures (*15*) (supporting online text). Additionally, a concentrated source of carbonate minerals may have been present and mechanically weathered and mixed with the other components of the dust. Extensive searches with TES and other spectroscopic measurements indicate that high concentrations of carbonates are not exposed on the martian surface at the ~10-km scale (*7–10*, *24*).

Carbonate minerals at concentrations of <5 weight % are common in the martian dust. The apparent wide distribution of carbonate minerals may be a large sink of a thicker past martian atmosphere. It is difficult to determine the total amount of CO_2 sequestered in martian carbonates because the vertical extent of carbonate minerals is not constrained. However, a global layer containing 2% carbonate 1 to 3 km thick can account for ~1 to 3 bars of CO_2 (*27*). Although the thickness of this layer is arbitrary, the presence of carbonates in the dust and martian meteorites indicates that carbonates occur on the martian surface and at depth. Carbonate formation on the martian surface would be dependent on the atmospheric pressure, thus serving as a mechanism that could develop and preserve the present martian atmospheric conditions.

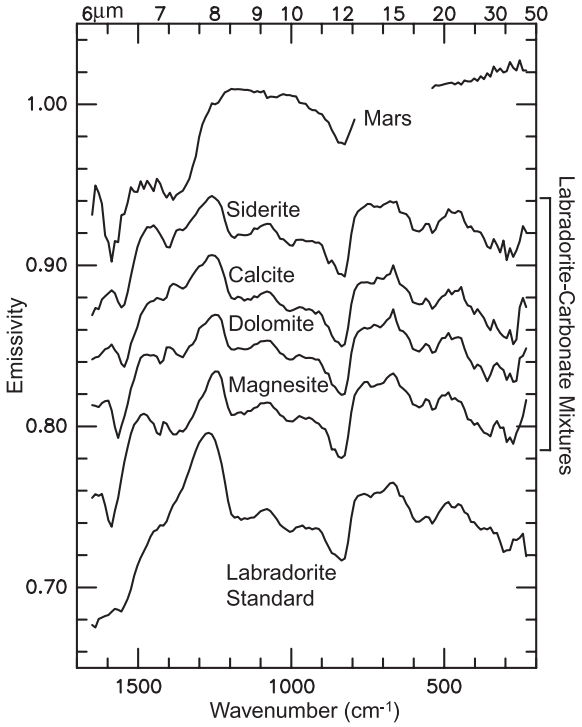

Fig. 3. Mars dust, labradorite standard, and labradorite-carbonate mixture spectra (offset). The position of the spectral features is dependent on the cation content of the carbonate.

References and Notes

1. M. C. Booth, H. H. Kieffer, *J. Geophys. Res.* **83,** 1809 (1978).
2. J. L. Gooding, *Icarus* **33**, 483 (1978).
3. V. C. Farmer, *The Infrared Spectra of Minerals* (Mineralogical Society, London, 1974).
4. J. W. Salisbury *et al.*, *Infrared (2.1–25 μm) Spectra of Minerals* (Johns Hopkins Univ. Press, Baltimore, 1991).
5. S. J. Gaffey *et al.*, in *Remote Geochemical Analysis: Elemental and Mineralogical Composition*, C. M. Pieters, P. Englert, Eds. (Cambridge Univ. Press, New York, 1993), pp. 43–71.
6. M. D. Lane, P. R. Christensen, *J. Geophys. Res.* **102**, 25581 (1997).
7. D. L. Blaney, T. B. McCord, *J. Geophys. Res.* **94**, 10159 (1989).
8. W. M. Calvin, T. V. King, R. N. Clark, *J. Geophys. Res.* **99**, 14659 (1994).
9. C. Wagner, U. Schade, *Icarus* **123**, 256 (1996).
10. P. R. Christensen *et al.*, *J. Geophys. Res.* **106**, 23823 (2001).
11. A. Banin, J. Rishpon, *J. Mol. Evol.* **14**, 133 (1979).
12. The reactivity of the soils was inconsistent with any large (>1 to 2%) abundance of Mg or Ca carbonate in the presence of smectite clays. There is no conclusive evidence for smectite clays in the martian soil and dust.
13. M. Settle, *J. Geophys. Res.* **84**, 8343 (1979).
14. R. L. Huguenin, *J. Geophys. Res.* **79**, 3895 (1974).
15. J. L. Gooding, *Icarus* **99**, 28 (1992).
16. J. L. Bandfield, M. D. Smith, *Icarus* **161**, 47 (2003).
17. Materials and methods are available as supporting material on *Science* Online.
18. S. W. Ruff, *Eos* **83**, 1059 (2002).
19. S. W. Ruff, P. R. Christensen, *J. Geophys. Res.*, 2001JE001580 (2002).
20. J. W. Salisbury, L. S. Walter, *J. Geophys. Res.* **94**, 9192 (1989).
21. B. H. Betts *et al.*, *J. Geophys. Res.* **100**, 5285 (1995).

22. B. M. Jakosky *et al*., *Geophys. Res. Lett.* **17**, 985 (1990).
23. Several investigations have tentatively identified carbonate absorptions in the atmospheric dust based on telescopic data sets (*31*, *32*). The number of spectra collected is limited and the large footprints include a wide range of surface temperatures, making the data difficult to interpret. These absorptions are inconsistent with Mariner 6/7 IRS, Mariner 9 IRIS, and MGS TES data, which all produce consistent spectral features and are considered well calibrated.
24. J. L. Bandfield, *J. Geophys. Res.*, 2001JE001510 (2002).
25. J. L. Bandfield, V. E. Hamilton, P. R. Christensen, *Science* **287**, 1626 (2000).
26. R. Kahn, *Icarus* **62**, 175 (1985).
27. F. P. Fanale *et al*., in *Mars*, H. H. Kieffer, B. M. Jakosky, C. W. Snyder, M. S. Matthews, Eds. (Univ. of Arizona Press, Tucson, 1992), pp. 1135–1179.
28. O. B. Toon, J. B. Pollack, W. Ward, K. Bilski, *Icarus*, **44**, 552 (1980).
29. F. P. Fanale, J. R. Salvail, W. B. Banerdt, R. S. Saunders, *Icarus* **50**, 381 (1982).
30. J. B. Pollack, J. F. Kasting, S. M. Richardson, K. Poliakoff, *Icarus* **71**, 203 (1987).
31. E. Lellouch *et al*., *Planet. Space Sci.* **48**, 1393 (2000).
32. J. B. Pollack *et al*., *J. Geophys. Res.* **95**, 14595 (1990).
33. We thank M. Kraft, M. Smith, J. Pearl, P. Niles, L. Leshin, V. Hamilton, A. Baldridge, and S. Ruff for discussions that significantly improved the manuscript. K. Bender, K. Homan, K. Murray, N. Gorelick, S. Anwar, and H. Moncrief provided operations and software support necessary for the TES investigation. R. Clark and an anonymous reviewer provided helpful discussion and comments that improved the clarity of the data presented here.

Supporting Online Material
www.sciencemag.org/cgi/content/full/301/5636/1084/DC1
Materials and Methods
SOM Text
Figs. S1 and S2

16 June 2003; accepted 18 July 2003

Tidally Controlled Stick-Slip Discharge of a West Antarctic Ice Stream

Robert A. Bindschadler,[1]* Matt A. King,[2] Richard B. Alley,[3] Sridhar Anandakrishnan,[3] Laurence Padman[4]

A major West Antarctic ice stream discharges by sudden and brief periods of very rapid motion paced by oceanic tidal oscillations of about 1 meter. Acceleration to speeds greater than 1 meter per hour and deceleration back to a stationary state occur in minutes or less. Slip propagates at approximately 88 meters per second, suggestive of a shear wave traveling within the subglacial till. A model of an episodically slipping friction-locked fault reproduces the observed quasi-periodic event timing, demonstrating an ice stream's ability to change speed rapidly and its extreme sensitivity to subglacial conditions and variations in sea level.

Concern that the West Antarctic Ice Sheet did, does, and will contribute to increasing sea level has driven two decades of extensive research on ice-flow dynamics (*1*, *2*). Evidence for periods of rapid retreat abounds (*3*–*5*). Currently northward-draining parts of this ice sheet are thinning rapidly, but not at rates sufficient to provide a large fraction of the present rate of sea level rise (*6*). The rest of the ice sheet is now close to equilibrium or slightly thickening (*7*, *8*).

For the West Antarctic Ice Sheet to raise sea level rapidly in the near future would require a substantial acceleration of its ice streams, the fast-moving rivers of ice that discharge much of the ice sheet back into the oceans (*9*). Some of these outlets are accelerating or have accelerated recently (*10*). Elsewhere, the major ice streams feeding the Ross Ice Shelf have either stopped, are decelerating, or are maintaining their velocity (*7*). In the case of Whillans Ice Stream (WIS), the current rate of deceleration is 1 to 2% per year, a rate that would result in stagnation if sustained over the next 50 to 100 years.

Recent field global positioning system (GPS) measurements from a 2-week survey on the "ice plain" in the mouth of WIS revealed that this portion of the ice stream moves by brief, rapid motion events separated by extended periods of no motion (*11*). Position solutions every 5 min illustrate this stick-slip motion of the ice plain (Fig. 1) (*12*). Quiescent periods were from 6 to 18 hours long. Slip events lasted from 10 to 30 min, during which the ice moved downstream a distance of a few tens of centimeters at rates of about 1 meter per hour, at least 30 times faster than the already high velocity of the ice stream feeding the ice plain. There was no measurable vertical motion associated with this phenomenon. For any particular site, flow reached approximately the same speed during each slip event. These speeds corresponded closely to the speeds calculated assuming a frictionless bed (*13*). Differential processing of GPS data for pairs of stations permitted a finer temporal view of the evolution of slip events (*14*). Acceleration to frictionless speeds was accomplished in as little as 30 s, the limiting temporal resolution. Deceleration was somewhat slower, but usually occurred within 2 to 5 min. Minor upstream rebound also was observed in the first hour of stagnation, typically amounting to about 10% of the downstream displacement.

Slip occurred across the ice plain, but was not exactly synchronous. Interpolation of slip displacements from the 5-min positions at up to five simultaneously occupied stations produced typical lags of a few minutes between the times of maximum speed. To quantify the speed and direction of this propagation effect, trios of sites were examined (*15*). From 17 sets of data, a mean speed of propagation of 88 $\pm$ 79 m/s was determined. This speed is close to the 150 m/s shear wave speed measured in the subglacial till farther upstream (*16*). The large uncertainty may represent some spatial heterogeneity in the propagation effect. The general direction of plane wave propagation was northward, nearly transverse across the ice plain, but there were significant variations from this direction. The propagation through the floating ice shelf is probably as a much faster-moving elastic body wave because the ice shelf coupling to water is inefficient (*17*).

A few deviations from stick-slip behavior were noticed, all at the edges of the ice plain (*18*). During periods of no motion on the ice plain, ice-shelf stations moved gradually downstream with larger displacements in synchrony with slips of the grounded ice plain. Occupation times at most sites were short, spanning only two to four slip events; therefore, a full characterization must await subsequent field studies.

There is a clear association between this stick-slip phenomenon and the ocean tide, which has a dominant diurnal component beneath the Ross Ice Shelf (*19*). During the survey, the tidal cycle ranged from weak, neap tides with a minimum amplitude of 0.15 m to a nearly 1-m amplitude during

[1]Ocean and Ice Branch, NASA Goddard Space Flight Center, Greenbelt, MD 20771, USA. [2]School of Civil Engineering and Geosciences, University of Newcastle, Newcastle Upon Tyne, NE1 7RU, UK. [3]Department of Geosciences and EMS Environment Institute, Pennsylvania State University, University Park, PA 16802, USA. [4]Earth and Space Research, Seattle, WA 98102–3620, USA.

*To whom correspondence should be addressed. E-mail: Robert.A.Bindschadler@nasa.gov